C. R. Chimie 19 (2016) 556–565

Contents lists available at ScienceDirect

Comptes Rendus Chimie

www.sciencedirect.com

Full paper/Mémoire

Benzoate liquid crystals with direct isotropic–smectic transition and antipathogenic activity

Daniela Ailincai [a], Luminita Marin [a, *], Sergiu Shova [a], Cristina Tuchilus [b]

[a] "Petru Poni" Institute of Macromolecular Chemistry of Romanian Academy, Grigore Ghica Voda Alley, No. 41A, 700487, Iasi, Romania
[b] "Grigore T. Popa" University of Medicine & Pharmacy, Pharmacy Faculty, Universitatii Street, No. 16, 700115, Iasi, Romania

ARTICLE INFO

Article history:
Received 30 October 2015
Accepted 21 January 2016
Available online 2 March 2016

Keywords:
Ester
Smectic liquid crystal
Wettability
Antipathogen

ABSTRACT

A smectogen liquid crystal based on benzoate units has been synthesized and structurally characterized by FTIR and ^{1}H NMR spectroscopy. Besides, its structure and supramolecular arrangement in the crystalline state was demonstrated by single crystal X-ray diffraction measurements. The thermotropic behaviour, monitored by differential scanning calorimetry and polarized light microscopy, consists in the formation of an enantiotropic smectic mesophase with a direct first order transition from the isotropic to smectic mesophase, and with its thermal stability range superposed on human body temperature. The smectogen liquid crystal has moderate wettability – suitable for biocompatible materials and presents good antipathogenic activity against gram positive and gram negative bacteria and fungus.

All these properties recommend the understudied liquid crystal to be used in biochemical and biological applications.

1. Introduction

Liquid crystals (LC) based on ester units are an interesting class of compounds which combine the anisotropic properties of the liquid crystals with the biological characteristics of the esters, promising to be a new class of biological relevant materials for surface functionalization [1], drug delivery systems [2], protein sorption/desorption [3], biological sensors [4], wound healing [5] membranes [6], gene therapy [7] and so on. A significant number of ester based liquid crystals have been mainly synthesized with the aim of being applied in optoelectronics and photonics as LC displays [8], field effect transistors [9], organic light emitting diodes [10], optical data storage devices [11], or photovoltaic cells [12]. Their application field is further enlarged by incorporating them into a polymeric matrix when systems known as polymer dispersed liquid crystals (PDLCs) are obtained [13]. The PDLC systems combine valuable properties of the two components and are designed for a wide range of applications, those in high performance biomedical field being especially envisaged in the last years, as artificial iris [14], blood sensors or sperm testers [15], smart packaging, and so on [16]. To be applied in such biological applications, liquid crystals must have the mesophase stability range at low temperature, eventually superposed on human body temperature. Moreover, speaking about the particular case of smectic liquid crystals, a direct isotropic–smectic transition is required, in order to reach a monomorphic stable mesophase capable of bistability [17].

Having all these in mind, we designed an ester based liquid crystal with a benzoate core and two aliphatic end groups which bring the benefits of the low temperature mesophase stability and of the direct isotropic–smectic transition. Besides, the ester groups provide the advantage of a potential biologically friendly compound, with real possibilities to be used in biochemistry and biological applications.

* Corresponding author.
E-mail address: lmarin@icmpp.ro (L. Marin).

http://dx.doi.org/10.1016/j.crci.2016.01.008
1631-0748/

2. Experimental

2.1. Reagents

4-Hydroxybenzoic acid ≥99%, butyl 4-hydroxybenzoate ≥99%, 1-bromooctane 99%, thionyl chloride 99%, anhydrous pyridine 99.8%, potassium hydroxide >85% were purchased from Aldrich and used as received. All the solvents of high purity were purchased from Carl Roth and used without any other purification.

2.2. Synthesis

The smectic liquid crystal has been synthesized using an input from published procedures [18] and optimized to the best yield, as can be seen in Scheme 1.

2.2.1. p-Octyloxy-benzoic acid (**2**)

In a round bottom flask, solutions of 4-hydroxybenzoic acid (1.1 g, 8 mmol) in 15 mL dry ethanol, and KOH (0.89 g, 16 mmol) in 5 mL dry ethanol were introduced, and over the resulted mixture *n*-bromooctyl (1 mL, 8 mmol) reagent was added drop wise, under vigorous stirring. The reaction mixture was refluxed for 14 h under nitrogen atmosphere, and then allowed to reach room temperature. The solid inorganic salts were removed by filtration and the pH of the resulted solution was adjusted to 2 by adding diluted HCl (0.1M). The crude product was filtered off, washed with water and recrystallized from acetic acid and then toluene, to give a white powder with a yield of 67%.

2.2.2. p-n-Octyloxy benzoyl chloride (**3**)

Thionyl chloride (1.5 g, 25 mmol) was added dropwise, at room temperature, to a solution of *p*-octyloxybenzoic acid (2.2 g, 13 mmol) in dimethylchloride (25 mL) with few drops of dimethylformamide, and the resulted mixture was stirred for 2 h. After that, the solvent was removed by distillation to give an ochre powder which was further used without any purification.

2.2.3. Butyl-p-[p′-n-octyloxy benzoyloxy]benzoate (***BBO***)

The final product butyl-*p*-[*p*′-*n*-octyloxy benzoyloxy] benzoate (**BBO**) was obtained by reaction of the *p*-*n*-octyloxy benzoyl chloride (**3**) with the commercial *p*-hydroxy butyl benzoate (**4**). The crude product has been recrystallized from ethyl acetate when fine white single crystals suitable for crystallographic measurements were obtained.

^{1}H NMR (400.13 MHz, DMSO-d_6, ppm) δ = 8.12, 8.10 (d, 2H, H3,H5); 8.09, 8.07 (d, 2H, H20,H22); 7.47, 7.45 (d, 2H, H19,H23); 7.16, 7.14 (d, 2H, H2,H6); 4.34, 4.32, 4.30 (t, 2H, H27); 4.13, 4.11, 4.10 (t, 2H, H8); 1.79, 1.77, 1.75, 1.74, 1.71 (m, 4H, H9,H28); 1.49, 1.47, 1.45, 1.44, 1.42 (m, 4H, H10,H29); 1.40–1.24 (overlapped peaks, 8H, H11,H12,H13,H14); 0.99, 0.97, 0.95 (t, 3H, H30); 0.91, 0.89, 0.87 (t, 3H, H15)

FTIR (KBr, cm^{-1}): 2954, 2921, 2855 (ν_{CH3}, ν_{CH2}), 1720 ($\nu_{C=O}$), 1602 ($\nu_{C=Caromatic}$), 1252 (ν_{C-O-C}), 845, 760 ($\delta_{CHaromatic}$).

Crystal data $C_{52}H_{68}O_{10}$ (M_r = 853.06 g mol^{-1}), triclinic, a = 5.7447(6) Å, b = 14.5648(14) Å, c = 28.725(2) Å, α = 98.673(7)°, β = 94.343(7)°, γ = 91.478(8)°; V = 2367.4(4) Å^3, T = 160 K, space group $P-1$, Z = 2, 1652 coll. refl., 8053 indep. (R_{int} = 0.0779), G_{of} = 1.000, R_1 = 0.0935, $wR(F^2)$ = 0.2132.

2.3. Equipment

Infrared (*IR*) spectrum of the solid **BBO** was recorded on a FTIR Bruker Vertex 70 Spectrophotometer in the transmission mode, by using KBr pellets.

^{1}*H-NMR spectrum* was recorded on a BRUKER Avance DRX 400 MHz spectrometer, equipped with a 5 mm direct detection QNP probe with *z*-gradients. The chemical shifts are reported as δ (ppm) relative to the residual peak of the DMSO solvent.

Crystallographic measurements on the **BBO** single crystal were carried out with an Oxford-Diffraction XCALIBUR E CCD diffractometer using graphite-monochromatic MoKα radiation, under the conditions described in the literature [19]. Crystallographic data for BBO have been deposited at the Cambridge Crystallographic Data Centre as Supplementary Publications No. CCDC-1416309. Copies of the data can be obtained free of charge from CCDC (12 Union Road, Cambridge CB2 1EZ, UK; Tel.: +44 1223 336 408; fax: +44 1223 336 033; e-mail: deposit@ccdc.cam.ac.uk; www:http://ccdc.cam.ac.uk).

The textures of the **BBO** liquid crystal were investigated by polarized light microscopy, with an Olympus BH-2 microscope equipped with a Linkam THMS 600/HSF9I heating stage and a TMS91 control unit. The samples were observed during a heating/cooling/heating scan, at a heating/cooling rate of 5 °C min^{-1}.

Differential scanning calorimetric (DSC) measurements were performed on a DSC 200 F3 Maia device (Netzsch, Germany), under nitrogen purge (nitrogen flow 50 mL/min). The device temperature and sensitivity was

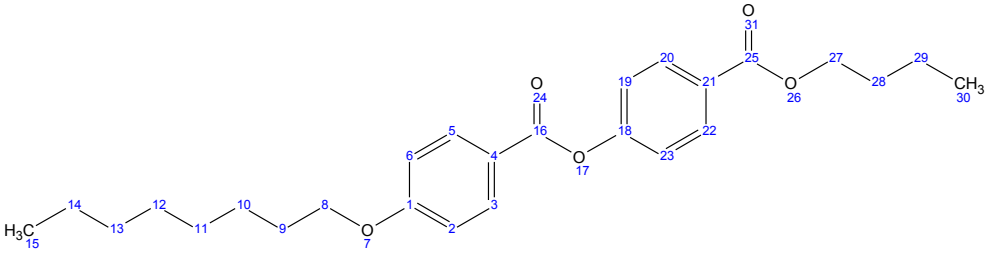

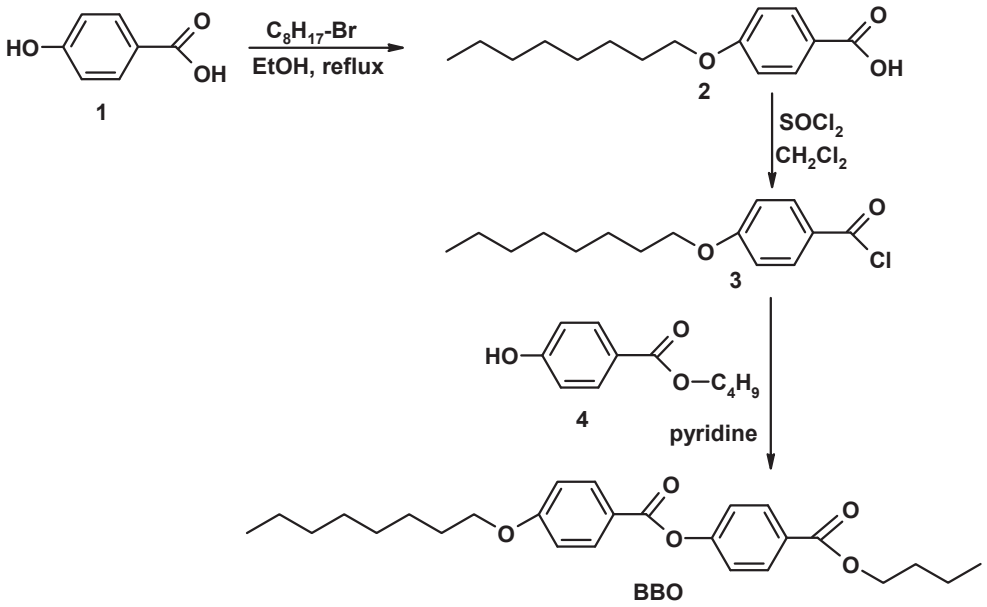

Scheme 1. Synthesis of **BBO** butyl-*p*-[*p*′-*n*-octyloxy benzoyloxy]benzoate.

calibrated with indium, according to the standard procedures. Around 5 mg of **BBO** sample was loaded in a punched and sealed aluminium crucible and DSC curves have been registered on a heating–cooling–heating scan, at a 5° C min^{-1} rate. The transition temperatures were read at the top of the endothermic and exothermic peaks.

The static contact angle for the **BBO** deposition was obtained using a CAM-200 instrument from KSV Finland, by the sessile drop method, at room temperature and controlled humidity. A drop of 1 μL was placed on the **BBO** film surface and the measurement was performed within 10 s. The contact angle was measured 5 times on random locations of the surface, the average value being considered. To calculate the components of the free surface energy and the total free surface energy, the contact angle at equilibrium between the studied surface and three pure liquids – twice distilled water, formamide and diiodomethane – was measured [16c,20].

The UV–vis absorption and photoluminescence spectra were recorded on a Carl Zeiss Jena SPECORD M42 spectrophotometer and Perkin Elmer LS 55 spectrophotometer respectively. The UV–vis spectrum of the **BBO** was registered in diluted chloroform solution ($\cong 10^{-5}$ %) using 10 mm quartz cells fitted with poly(tetrafluoroethylene) stoppers. The photoluminescence spectrum of the **BBO** was obtained by exciting the film with a light wavelength corresponding to the absorption maximum.

The antimicrobial activity of the **BBO** compound was evaluated against both gram positive and gram negative bacteria and also against fungus, using the agar diffusion method [21]. The used microorganisms were: *Staphylococcus aureus ATCC 2592 and Sarcina lutea ATCC 9341* gram positive bacteria; *Escherichia coli ATCC 25922* and *Pseudomonas aeruginosa* ATCC 27853 gram negative bacteria; and *Candida albicans* ATCC 10231, *Candida glabrata ATCC MYA 2950* and *Candida parapsilosis* ATCC *22019* fungus. Stainless steel cylinders, with an inner diameter of 6 mm, were placed in Petri dishes containing Mueller-Hinton agar medium for bacteria, and Sabourand medium for fungus. The medium (Oxoid, UK) was inoculated with the microorganism suspension. Afterwards, the cylinders were filled with 100 μl solution of **BBO** in DMSO (10 mg/mL). After incubation at 37 °C for 24 h, the diameter of the inhibition zone was measured. The results are expressed as the mean value of three different measurements. Two disks, one of 25 μg ampicillin and one of 30 μg chloramphenicol were used as etalons for the antimicrobial activity, while a disk of myconazol of 50 μg, and one of nystatin of 100 μg were used as etalons for the antifungal activity.

3. Results and discussions

3.1. Synthesis and structure

A thermotropic smectic liquid crystal containing ester linkages named butyl-*p*-[*p*′-*n*-octyloxy benzoyloxy]benzoate] (**BBO**) has been synthesized by an esterification reaction starting from *p*-hydroxy benzoic acid (Scheme 1). The right structure of the liquid crystal has been proved by ^{1}H NMR and FTIR spectroscopy and further by single crystal X-ray diffraction measurements.

The FTIR spectrum of the **BBO** revealed all the characteristic absorption bands of the new formed compound, confirming the reaction pathway. Thus, in the finger print region, significant bands are seen at 1720 cm^{-1} assigned to the stretching vibration of COO groups and at 1602 cm^{-1} attributed to the stretching vibration of the double bond in the aromatic ring. Symmetric and anti-symmetric stretching vibrations of the C–H bond of CH_2 and CH_3 units are also present at 2954, 2921 and 2855 cm^{-1} (Fig. 1).

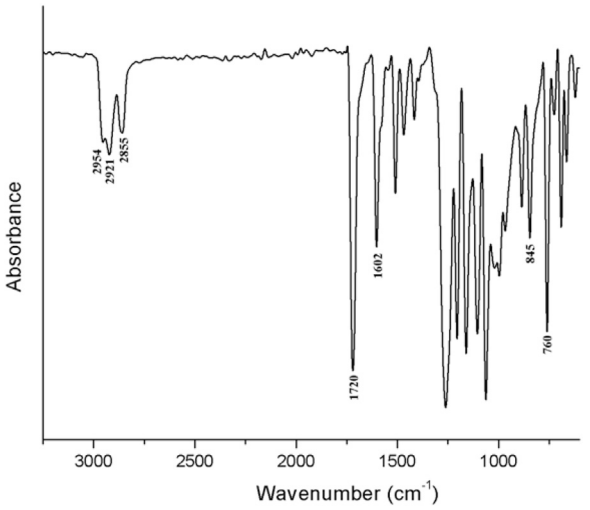

Fig. 1. FTIR spectrum of the **BBO** liquid crystal.

Further, the NMR spectrum of the **BBO** exhibits all the chemical shifts characteristic of the aromatic and aliphatic protons, in the right integral ratio, confirming the right structure and the high degree of purity (Fig. 2).

Single crystal X-ray diffraction of the **BBO**, clearly indicated the targeted structure and moreover, gave a view on the driving forces to the supramolecular arrangement of the molecules in the crystal structure. Fig. 3 presents a perspective view of two crystallographic independent but chemically identical molecules as the asymmetric part of the unit cell. Both molecules (**A** and **B**) exhibit very close geometric parameters listed in Table 1S.

The crystal structure essentially results from the packing of two-dimensional layers parallel to the (110) plane. A fragment of the crystal structure viewed along the *a* axis is shown in Fig. 4. Each layer has a thickness of approximately 27 Å, being constructed due to the antiparallel arrangement of the asymmetric molecules **A** and **B** along the *c* crystallographic axis. There are two types of inter-molecular interactions, which caused the formation of supramolecular layers: molecules **A** and **B** in an antiparallel orientation are linked through short contacts, evidenced for numerous (i) π–π, and (ii) C–H···π interactions (Fig. 5) [22]. In addition, along the perpendicular direction the supramolecular layers are additionally sustained *via* a system of similar C–H···O inter-molecular hydrogen bonding comprising separately A and B molecules. As an example, the H-bondings which occur between molecules A are shown in Fig. 6.

This bonding network facilitates a rigid-flexible self-assembly which further plays an important role in the thermotropic behaviour.

3.2. Liquid crystalline behaviour

The thermotropic behaviour of the **BBO** has been firstly monitored by differential scanning calorimetry. As can be seen in Fig. 7, during the heating scans, two endothermic peaks – a more intense one at 54 °C (~ 80 J/g) and a less intense one at 70 °C (15.38 J/g) – indicate the presence of a

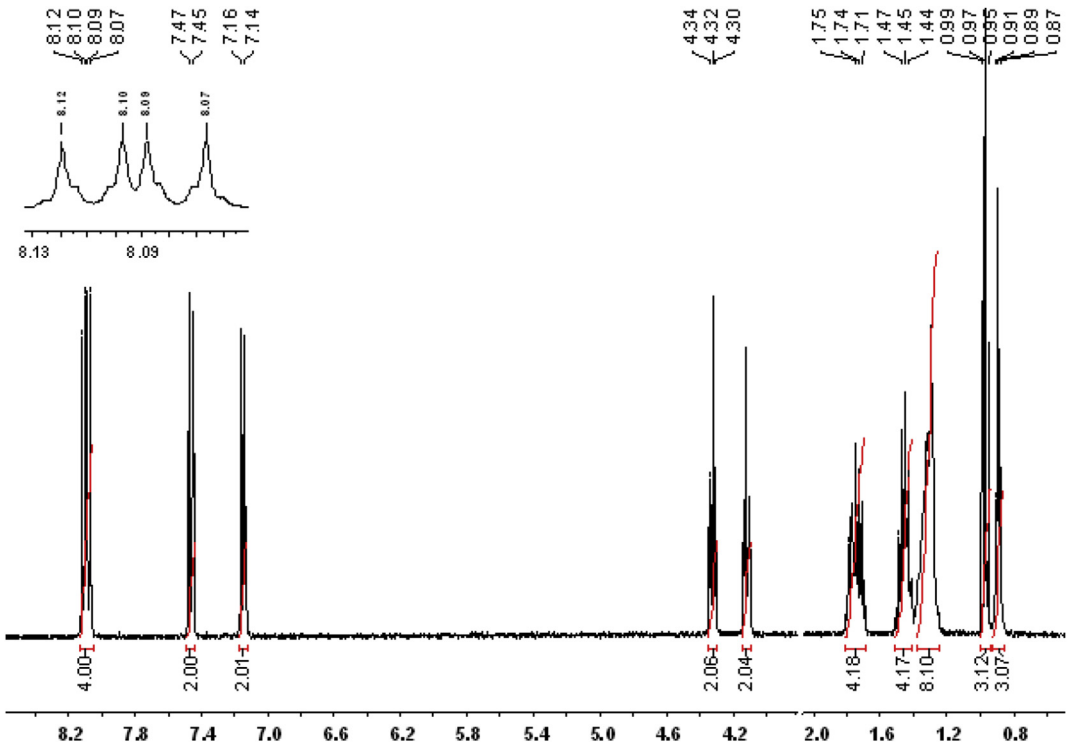

Fig. 2. NMR spectrum of the **BBO** liquid crystal.

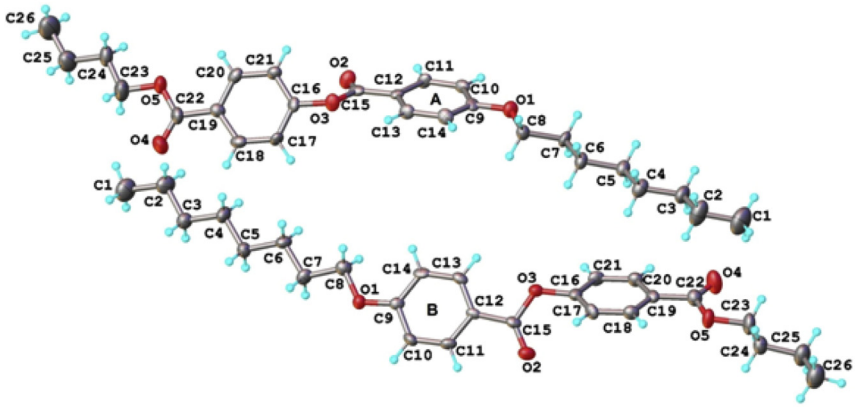

Fig. 3. Two crystallographic independent molecules (**A** and **B**) in the asymmetric part of the unit cell. Thermal ellipsoids are drawn at 50% probability level.

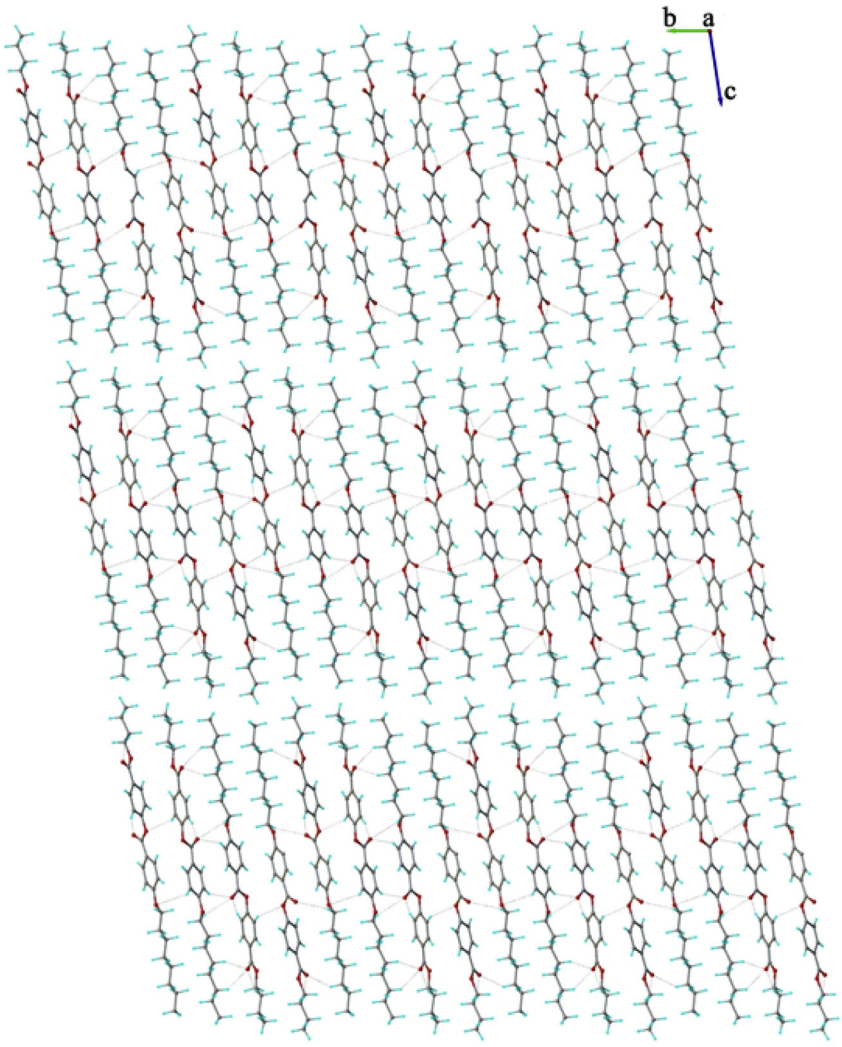

Fig. 4. The crystal structure of the **BBO** viewed along the *a* axis.

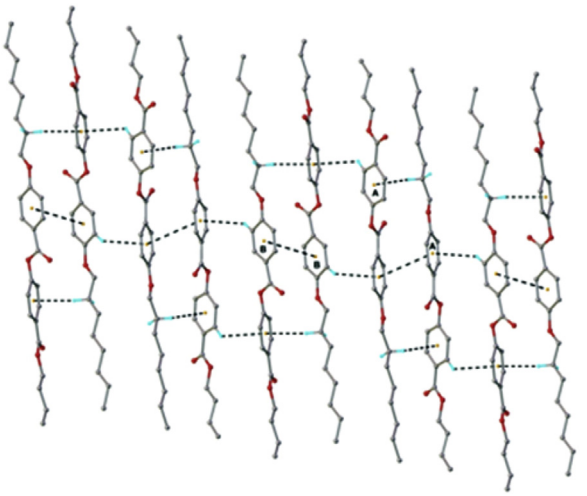

Fig. 5. View of the crystal structure showing (i) π–π, and (ii) C–H···π interactions in the crystal structure of the **BBO**. The centroid-to-centroid and C–H···π distances are in the range of 3.885÷3.892 Å and 2.759÷2.993 Å, respectively.

mesophase. In the cooling scans, in a reverse manner, two exothermic peaks occur too, at 69 °C (−15,51 J/g) and 29 °C (−68.08 J/g), respectively. The enthalpy change of the exothermic processes has similar value with that of the corresponding endothermic processes. Taking into consideration the high values of enthalpy changes, it can be assumed that **BBO** forms an enantiotropic smectic mesophase, being known that smectic–isotropic transition involves more energy compared to the nematic-isotropic one [23]. The high hysteresis of the lower temperature transition is characteristic of a difficult crystallization process

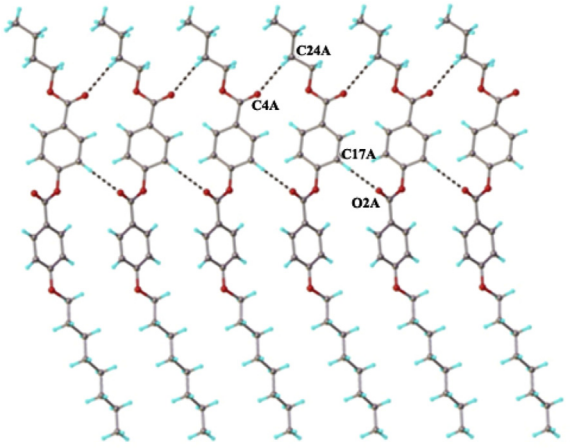

Fig. 6. C–H···O hydrogen bonding within the two-dimensional layer. H-bond parameters: C17A–H···O2A [C17A–H 0.93 Å, H···O2A 2.42 Å, C17A···O2A(−1 + *x*, *y*, *z*) 3.333(6) Å, C17A–H···O2A 166.1°]; : C24A–H···O4A [C24A–H 0.97 Å, H···O4A 2.65 Å, C24A···O2A(1 + *x*, *y*, *z*) 3.568(67) Å, C24A–H···O2A 157.2°]; C21B–H···O2B [C21B–H 0.93 Å, H···O2B 2.41 Å, C21B···O2B(1 + *x*, *y*, *z*) 3.303(6) Å, C21B–H···O2B 162.0°]; C24B–H···O4B [C24B–H 0.97 Å, H···O4B 2.54 Å, C24B···O4B(-1 + *x*, *y*, *z*) 3.472(6) Å, C24B–H···O4B 160.7°].

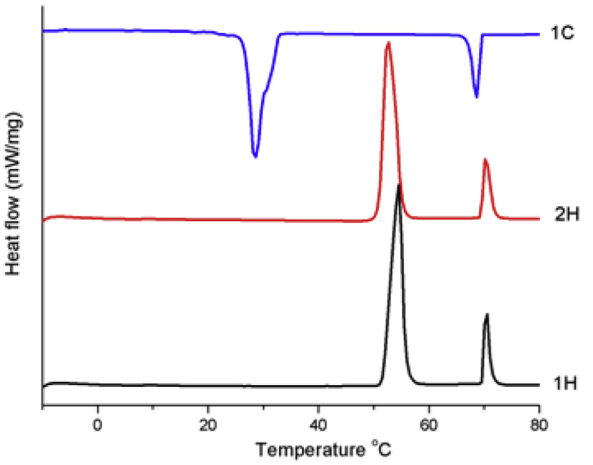

Fig. 7. DSC curves of the butyl-*p*-[*p*′-*n*-octyloxy benzoyloxy]benzoate.

from the viscous smectic fluid into the complex crystalline structure, most probably due to the weaker H-bond interactions among the supramolecular layers, related to their low dipole moment [24].

To gain deeper insight into the mesophase type, polarized light microscopy (POM) was performed under similar conditions with DSC measurements. Under polarized light, at room temperature, the **BBO** shows strong birefringent needle crystals (Fig. 8a). During the first heating cycle, the needle-like crystals suffered a transition to a fluid, striated marble texture difficult to be ascribed (Fig. 8b), which further became isotropic. The two transitions occurred at temperatures corresponding to the DSC endotherms. In the cooling scan, from the isotropic fluid, a clear fan shape texture, characteristic of the smectic A mesophase appeared (Fig. 8c), and crystallized at further cooling (Fig. 8d). Both transitions occurred at temperatures corresponding to the DSC exotherms. No other transition could be observed before crystallization, even after decreasing the cooling speed to 3, 1, or 0.1 °C min^{-1}. It can be remarked that the smectic mesophase formed during the cooling is stable on a larger temperature range (40 °C) compared to that occurred during the heating (16 °C).

Taking into consideration the crystalline structure as demonstrated by single crystal X-ray diffraction, the formation of the smectic mesophase was explained by the tendency of the **BBO** molecules to form layered structures by rigid-flexible segregation, which appeared to be the principal driving force in keeping crystal integrity. As the temperature increased the weaker H-bonds interactions were destroyed and the σ bonds of the flexible spacer gained enough energy to rotate competing with the π–π and C–H···π cohesion forces between the rigid parts, and thus a smectic mesophase was formed. As the temperature increased more, the molecules gained enough energy for translational moving, and thus the layered ordering of the smectic mesophase was lost. The direct smectic–isotropic transition without a transition *via* a nematic mesophase, appeared to be the result of the short inter-molecular distances and consequently strong inter-molecular forces

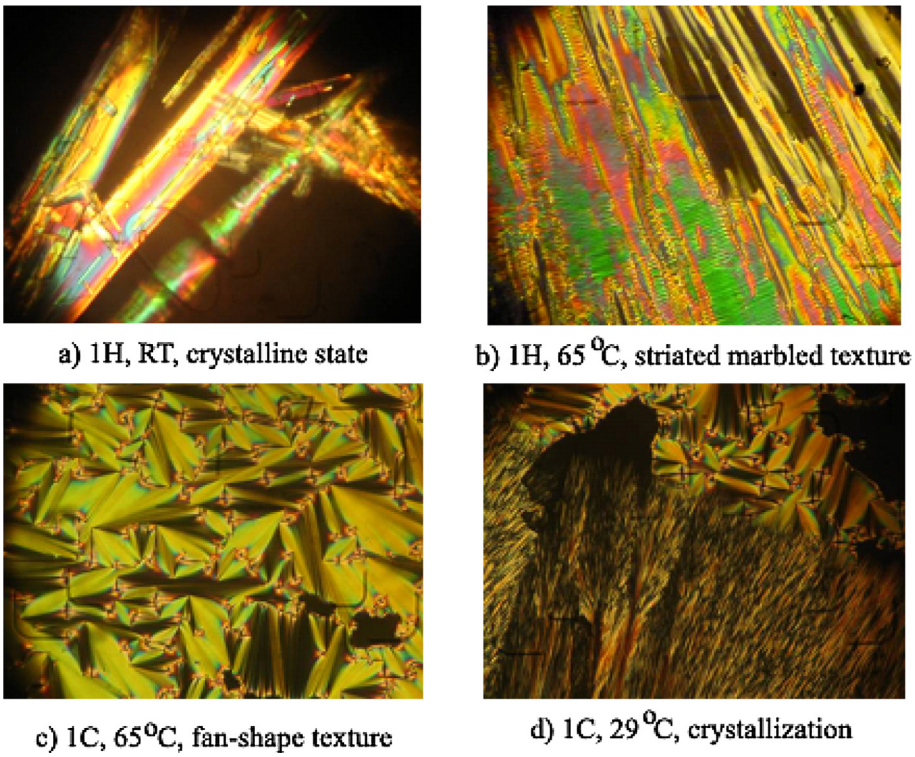

Fig. 8. POM images revealing thermotropic behaviour of the **BBO** smectic liquid crystal.

between the rigid cores. This kind of interaction was completely vanished by increasing the temperature at a value at which the molecules gained enough energy for translational moving. In the cooling scan, the smectic mesophase appeared directly from the isotopic state, due to the strong π–π and C–H···π cohesion forces between the rigid cores which favoured the layer formation.

Comparing the data from the three methods (single crystal X-ray diffraction, POM and DSC), it can be concluded that the **BBO** ester based compound is a smectic liquid crystal with a direct isotropic–smectic transition and large mesophase stability range superposing with human body temperature. The smectic mesophase appears due to the tendency of BBO to aggregate in layered structures because of rigid-flexible self-assembling. The short inter-molecular distances indicate strong inter-molecular forces which disfavour the **BBO** molecule arrangement in a nematic mesophase and, on the other hand, favour the molecule arrangement in a layered structure and the direct isotropic–smectic transition. Besides, considering the biologically friendly building blocks [18a,b] used for obtaining **BBO** , the new liquid crystal appears to have potential use in biomedical applications.

3.3. Photophysical properties

The absorption behaviour of the **BBO** liquid crystal was studied in diluted solution of chloroform (10^{-5} M), when no interactions between molecules are possible and so they can be considered isolated. As can be seen in Fig. 9a, the **BBO** liquid crystal shows an absorption band with a maximum around 266 nm in the UV–vis spectrum, characteristic of the π–π benzenoid transition. By exciting with light of wavelength corresponding to the absorption maximum, the **BBO** film exhibits a large emission band expanding from the UV to green light domain (Fig. 9b), with emission maxima lying in principal in the blue light domain. The emission profile has a structured shape indicating the crystallization in crystals of different size and in different amounts. It is important to underline that no superposing of the absorption and emission bands was registered, pointing to no reabsorption phenomena and consequently potential use in biochemical and biological applications [25].

3.4. Surface characteristics

As the surface of a material is the first coming into contact with biological fluids, its characteristics in terms of wettability and surface energy are very important parameters when the level of biocompatibility of a material is investigated. The water contact angle of the **BBO** liquid crystal has the medium value of 68.4 degree which is comprised in the moderate wettability range of 60–90 degree – characteristic of the biocompatible materials [16,19,26]. Moreover, this contact angle value is close to the value of 60 degree of the corneal surface [27] indicating the BBO as potential candidate for ocular biomedical applications.

The **BBO** liquid crystal based on benzoate units has high surface energy value of 42.8 mN/m, given by higher dispersive Lisfshitz – van der Waals contribution

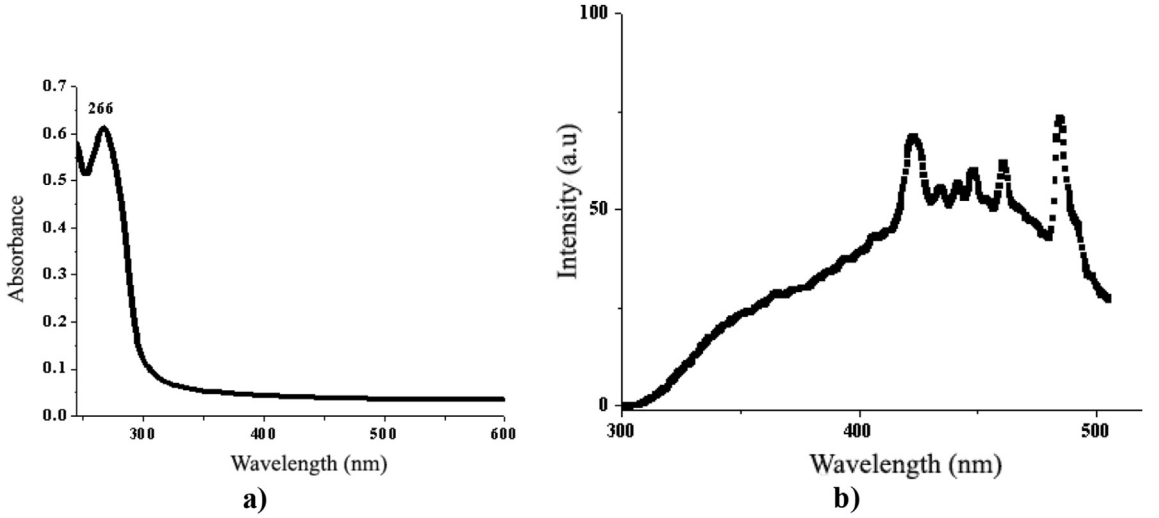

Fig. 9. a) UV–vis and b) photoluminescence spectra of the **BBO**.

($\gamma_S^{LW} = 40.32$) and less important polar forces ($\gamma^a = 2.48$) as result of almost missing electron accepting ($\gamma_S^+ = 0.08$) contributions despite important electron donating ($\gamma_S^- = 18.22$) contribution. This is in agreement with the structure of the **BBO** consisting of electron rich ester groups and nonpolar aliphatic units. The surface energy value of the **BBO** liquid crystal is higher than 22 mN/m – value over which the cellular adhesion and the maintainance of the tissue multicellular structure was demonstrated to be favoured [28].

3.5. Antipathogenic tests

As the **BBO** compound was designed for being used in biomedical applications, a preliminary screening of its antimicrobial activity was performed against common and virulent pathogen agents related to human healthcare, such as *S. aureus ATCC 25923* and *S. lutea ATCC 9341* gram positive bacteria, *E. coli ATCC 25922* and *P. aeruginosa* ATCC 27853 gram negative bacteria and *C. albicans* ATCC 10231, *C. glabrata ATCC MYA 2950* and *C. parapsilosis* ATCC *22019* fungus.

The antimicrobial activity was measured by the agar diffusion method in Petri dishes containing Mueller-Hinton agar medium for bacteria, and Sabourand medium for fungus. Except *P. aeruginosa*, the **BBO** liquid crystal exhibited strong antimicrobial activity against all the tested microorganisms, as can be observed in Fig. 10. Representative images of the inhibition area could be observed in Fig. 11.

Firstly, it can be observed that **BBO** reduces the culture of viable gram positive *S. aureus* and *S. lutea* bacteria on a large area around, with an inhibition zone about 15 mm, activity comparable with that of sugar fatty acid esters used as multifunctional food additives in food industries [29]. A plausible explanation of this good activity could be given taking into consideration the chemical structure of both interacting components. Thus, the cell surface of the gram positive bacteria contains lipoteichoic acid which could react with the ester groups of the BBO *via* a transesterification reaction. This should disrupt the membrane function and thus inhibit the culture growth.

Related to the gram negative bacteria, stagnation of the bacterial growth was observed only in the case of *E. coli*, while no activity could be seen against *P. aeruginosa.* This observation comes in line with other reported data which evidenced the catabolic activity of *P. aeruginosa* against a large variety of organic molecules including benzoates [30]. The good activity of the **BBO** against *E. coli* is remarkable, taking into consideration the high resistance of this bacterium to antibiotics [31].

Considerable activity of the **BBO** liquid crystal was also observed against fungus. Inhibition zone diameter between 14 and 19 mm for the three tested *Candida* fungus competes with the one obtained for the used Nystatin etalon – a well-known antifungal agent.

4. Conclusions

A smectogen liquid crystal based on benzoate units has been designed and successfully synthesised. The liquid

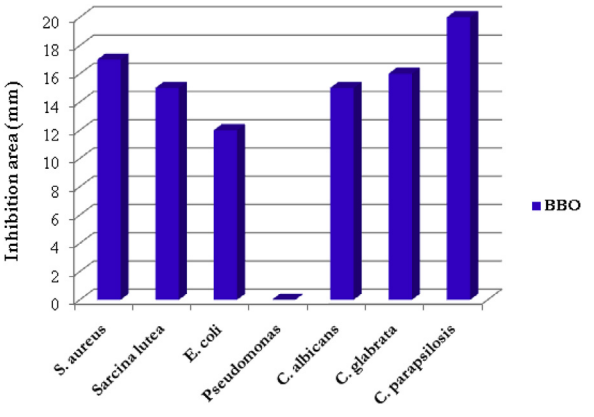

Fig. 10. The inhibition area (mm) of the **BBO** liquid crystal.

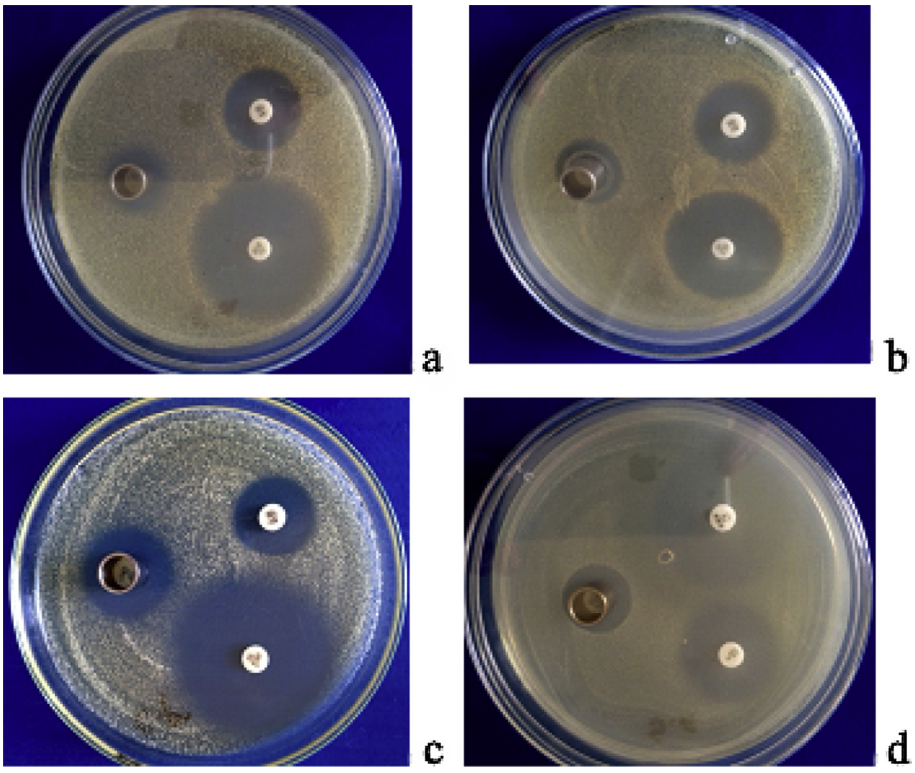

Fig. 11. The antimicrobial activity of the **BBO** liquid crystal against a) *Candida albicans*, b) *Candida glabrata*, c) *Candida parapsilosis*, d) *Staphilococus aureus*.

crystal has a direct isotropic–smectic transition and its thermal stability mesophase range superposes on human body temperature. The liquid crystal has excellent anti-pathogenic activity and its surface properties in terms of wettability and surface energy indicate it as a potential biocompatible material.

Acknowledgements

This work was financially supported by the Romanian National Authority for Scientific Research, MEN – UEFISCDI grant, project number PN-II-ID-PCCE-2011-2-0028 (4/2012) and project number PN-II-RU-TE-2014-4-2314 (72/2015).

Appendix A. Supplementary data

Supplementary data related to this article can be found at http://dx.doi.org/10.1016/j.crci.2016.01.008.

References

[1] C.F. Soon, W.I.W. Omar, F.R. Berends, N. Nayan, H. Basri, K.S. Tee, M. Youseffi, N. Blagden, M.C.T. Denyer, Micron 56 (2014) 73–79.
[2] (a) S. Milak, A. Zimmer, Int. J. Pharm. 478 (2015) 569–587;
(b) P. Saulnier, N. Anton, B. Heurtault, J.P. Benoit, C. R. Chimie 1 (2008) 221–228.
[3] P. Liu, W. Gao, Q. Zhang, K. Chen, J. Zhang, L. Chen, X. Zhang, K. Wang, React. Funct. Polym. 89 (2015) 1–8.
[4] B. Wu, K. Chen, Y. Deng, J. Chen, C. Liu, R. Cheng, D. Chen, Chem. Eur. J. 21 (2015) 3671–3681.
[5] (a) C.F. Soon, M. Youseffi, R.F. Berends, N. Blagden, M.C.T. Denye, Biosens. Bioelectron. 39 (2013) 14–20;
(b) Y. Bouligand, C. R. Chimie 11 (2008) 281–296;
(c) M.-M. Giraud-Guille, E. Belamie, G. Mosser, C. Helary, F. Gobeaux, S. Vigier, C. R. Chimie 11 (2008) 245–252.
[6] W. Han, M. Tu, R. Zeng, J. Zhao, C. Zhou, Carbohydr. Polym. 90 (2012) 1353–1361.
[7] C.R. Safinya, K. Ewert, A. Anmad, H.M. Evans, U. Raviv, D.J. Needleman, A.J. Lin, N.L. Slack, C. George, C.E. Samuel, Philos. T. Roy. Soc. A 364 (2006) 2573–2596.
[8] M. Matsui, S. Okada, M. Kadowaki, M. Yamada, Liquid Cryst. 29 (2002) 707–712.
[9] L.A. Tatum, C.J. Johnson, A.A.P. Fernando, B.C. Ruch, K.K. Barakoti, M.A. Alpuche-Aviles, B.T. King, Chem. Sci. 3 (2012) 707–712.
[10] A. Iwan, D. Pociecha, A. Sikora, H. Janeczek, M. Wegrzyn, Liq. Cryst 37 (2010) 1479–1492.
[11] S.M. Gan, A.R. Yuvaraj, M.R. Lutfor, M.Y. Mashitah, H. Gurumurthy, RSC Adv. 5 (2015) 6279–6285.
[12] A. Iwan, A. Sikora, V. Hamplová, A. Bubnov, Liquid Cryst. 42 (2015) 964–972.
[13] (a) S. Bronnikov, S. Kostromin, V. Zuev, J. Macromol. Sci.B 52 (2013) 1718–1735;
(b) L. Marin, E. Perju, Phase Transit. 82 (2009) 507–518;
(c) Y. Tu, Y. Gu, R.M. Van Horn, M. Mitrokhin, F.W. Harris, S.Z.D. Cheng, Polym. Chem. 6 (2015) 2551–2559.
[14] J. Lapointe, J.-F. Durette, A. Harhira, A. Shaat, P.R. Boulos, R. Kashyap, Eye 24 (2010) 1716–1723.
[15] Y.H. Lin, T.Y. Chu, Y.S. Tsou, K.H. Chang, Y.P. Chiu, Appl. Phys. Lett. 101 (2012) 233.
[16] (a) E. Perju, L. Marin, V.C. Grigoras, M. Bruma, Liq. Cryst 38 (2011) 893–905;
(b) L. Marin, M.C. Popescu, A. Zabulica, H. Uji-I, E. Fron, Carbohydr. Polym. 95 (2013) 16–24;
(c) L. Marin, D. Ailincai, E. Paslaru, RSC Adv. 4 (2014) 38397–38404.
[17] Y. Lu, J. Wei, Y. Shi, O. Jin, J. Guo, Liq. Cryst 40 (2013) 581–588.
[18] (a) A.V. Doshi, C.G. Joshi, U.C. Bhoya, Der Pharma Chemica 3 (2011) 185–190;
(b) Y.Z. Qiang, Y.C. Dong, Sci. Bull. 58 (2013) 2557–2562;
(c) J.M. Lohar, A.V. Doshi, J. Inst. Chem. 65 (1993) 15–17.

[19] (a) M.F. Zaltariov, M. Cazacu, N. Vornicu, S. Shova, C. Racles, M. Balan, C. Turta, Supramol. Chem. 25 (2013) 490–502;
(b) M.F. Zaltariov, M. Alexandru, M. Cazacu, S. Shova, G. Novitchi, C. Train, A. Dobrov, M.V. Kirillova, E.C.B.A. Alegria, A.J.L. Pombeiro, V.B. Arion, Eur. J. Inorg. Chem. 29 (2014) 4946–4956;
(c) M.F. Zaltariov, A. Vlad, M. Cazacu, S. Shova, M. Balan, C. Racles, Tetrahedron 70 (2014) 2661–2668.
[20] L. Marin, D. Ailincai, M. Mares, E. Paslaru, M. Cristea, V. Nica, B.C. Simionescu, Carbohydr. Polym. 117 (2015) 762–770.
[21] P.A. Wayne, CLSI document M100-S24, Vol. 1, Clinical and Laboratory Standards Institute, 2014, p. 34.
[22] (a) L. Marin, A. van der Lee, S. Shova, A. Arvinte, M. Barboiu, New J. Chem. 39 (2015) 6404–6420;
(b) Y. Liu, G. Zhan, X. Zhong, Y. Yu, W. Gan, Liq. Cryst 38 (2011) 995–1006;
(c) S. Noriko, H. Kayako, Liq. Cryst 28 (2001) 77–88.
[23] J.L. Serrano, P. Romero, M. Marcos, P.J. Alonso, J. Chem. Soc. Chem. Commun. 12 (1990) 859–861;
(b) I. Campoy, C. Marco, M.A. Gomez, J.G. Fatou, Polym. Bull. 27 (1991) 81–88;
(c) L. Marin, S. Destri, W. Porzio, F. Bertini, Liq. Cryst 36 (2009) 21–32.
[24] T.P. Stepanova, A.E. Bursian, V.M. Denisov, Phys. Solid State 44 (2002) 1993–2000.
[25] P. Horváth, P. Šebej, T. Šolomek, P. Klán, J. Org. Chem. 80 (2015) 1299–1311.
[26] E. Perju, E. Paslaru, L. Marin, Liq. Cryst 42 (2015) 370–382.
[27] R.M. Shanker, I. Ahmed, P.A. Bourassa, K.V. Carola, Int. J. Pharm. 119 (1995) 149–163.
[28] N. Hallab, K. Bundy, K. O'Connor, R.L. Moses, J.J. Jacobs, Tissue Eng. 7 (2001) 55–71.
[29] L. Zhao, H. Zhang, T. Hao, S. Li, Food Chem. 187 (2015) 370–377.
[30] A. Bazire, F. Diab, M. Jebbar, D. Haras, J. Ind. Microbiol. Biot. 34 (2007) 5–8.
[31] (a) R.S. Gupta, Microbiol. Mol. Biol. Rev. 62 (2000) 1435–1491;
(b) R.S. Gupta, Crit. Rev. Microbiol. 26 (2000) 111–131;
(c) M. Desvaux, M. Hébraud, R. Talon, I.R. Henderson, Trends Microbiol. 17 (2009) 139–145.